IIETA International Information and Engineering Technology Association
Advancing the World of Information and Engineering

Journal Européen des Systèmes Automatisés
Vol. 59, No. 5, May, 2026, pp. 1501-1514
Journal homepage: http://iieta.org/journals/jesa

Balanced Truncation-Based Model Order Reduction for MIMO Microgrid Systems

Minh-Cuong Nguyen[1,2]

[1] Education Technology and Adaptive Learning Institute, Thai Nguyen University of Technology, Thai Nguyen 24000, Vietnam
[2] Faculty of Electrical Engineering, Thai Nguyen University of Technology, Thai Nguyen 24000, Vietnam

Corresponding Author Email: nmc.etali@tnut.edu.vn

https://doi.org/10.18280/jesa.590525

Received: 27 October 2025
Revised: 10 December 2025
Accepted: 16 December 2025
Available online: 31 May 2026

Keywords:
balanced truncation, H∞ error analysis, MIMO microgrid, model order reduction, system dynamics

ABSTRACT

This study examines balanced truncation applied to a linearized multi-inverter microgrid represented by a 14-state dq model obtained at the nominal operating point of 50 Hz and rated steady-state voltage. The objective is to determine how model order affects the accuracy of dynamic behavior when reducing the full model to lower orders. The reduction is performed for orders from 1 to 13 and focuses on orders 4 and 8. The H∞ evaluation shows that the order 4 model yields errors close to 1.2×10^{-3} for channels driven by Inputs 1 and 2 toward Outputs 1 and 2, yet errors exceed 10 for channels associated with Inputs 3 and 4, indicating the loss of significant modes. The order-8 model produces errors ranging from 3.1×10^{-4} to 2.2×10^{-3} across all channels and preserves transient and frequency responses observed in impulse and Bode analyses. The findings suggest that order-4 may serve applications with limited channel interest while order-8 provides broader fidelity with reduced computational burden. The results offer a quantitative guideline for selecting reduced-order models in multi-inverter microgrid simulations and control studies.

1. INTRODUCTION

Microgrids play an important role in the context of energy transition and smart operation since they integrate distributed generation units, storage devices, and local loads into controllable electrical networks that can operate in islanded mode. When several converters interact through a common network the overall dynamics often take the form of a multiple input multiple output structure with several coupled state variables. Such a structure is central to voltage regulation, power sharing, and stability assessment in modern microgrids because it links local control actions with system level performance under changing operating conditions and disturbances [1].

The increasing penetration of renewable sources, advanced storage technologies, and hierarchical controllers drives microgrid models toward higher orders. Detailed representations that capture inner control loops, virtual impedance, and network dynamics can involve many states and several control inputs and outputs [1, 2]. These features improve accuracy but make analysis, simulation, and controller design more demanding. Time domain studies with many scenarios or frequency domain evaluations over a wide range of operating points require repeated evaluations of models that may contain more than ten states and several control channels [2, 3]. This situation motivates the use of reduced order models that preserve the dominant dynamic behavior while easing computational effort.

Model order reduction has become a widely used tool in this context since it provides simpler models that approximate the response of high order systems in a controlled way [3]. Examples include reduced order representations of converters with droop and virtual impedance [1], soft robotic structures governed by finite element models [2], and linear active disturbance rejection controllers that benefit from more compact dynamic descriptions [3, 4]. Other works present techniques that combine structural methods and performance indices to reduce system order while keeping stability and limiting integral errors such as Integral of Time-weighted Absolute Error (ITAE), Integral of Absolute Error (IAE), and Integral of Squared Error (ISE) [4, 5]. Studies on electromagnetic field problems and delayed wind energy frequency control also employ reduced order models to decrease the gap between detailed and simplified dynamics in a systematic way [5, 6]. Model order reduction has further been applied to high pressure heavy water reactor models and parameterized large scale circuit descriptions for VLSI applications where the number of states can be very large [7, 8]. Hybrid schemes based on classical approximations and moment-based approaches have been proposed to generate stable reduced models for complex mechanical systems [9, 10]. In power electronics and control, several contributions exploit time domain parameters, Markov data, or meta heuristic optimization to tune reduced order models and to minimize integral error criteria for converters and related systems [11, 12].

Within this broad family of methods, balanced truncation stands out as a reliable and conceptually clear approach for

linear time invariant systems [13]. The method relies on controllability and observability Gramians to transform the state space model into a balanced coordinate frame in which each state has an associated Hankel singular value that measures its joint contribution to input to state and state to output transmission [13, 14]. States with small Hankel singular values can then be discarded to form a reduced model while stability is preserved and error bounds are available [14, 15]. Balanced truncation has been applied to phase locked loop models in wind farm synchronization studies, to dynamic systems with special forms of outputs, and to switching systems with known switching sequences where time varying Gramians help construct reduced switching models [14-16]. In digital signal processing the method supports dedicated algorithms for finite impulse response multiple input multiple output filters and helps reduce their computational cost while keeping high accuracy [17]. Further works investigate adaptive order selection, compression of deep learning models on embedded platforms, and combinations with meta heuristic procedures in order to handle complex electrical networks and to extract informative error features for grid connected power electronic systems [18-21]. These studies confirm that balanced truncation can reduce model complexity in many application domains while keeping the essential dynamic characteristics of the original systems [13, 21].

Despite this progress the literature still provides limited insight into how balanced truncation behaves when applied to multi-inverter islanded microgrids that are modeled as coupled multiple input multiple output systems. Existing works that use model order reduction in converter control or networked power electronic systems often focus on specific controllers or device level models and rarely present a systematic scan of the reduced order together with a channel wise error analysis [1, 3, 4]. In particular the sensitivity of different output buses to truncation has not been quantified in a way that can guide practitioners in the selection of a suitable reduced order for microgrid simulation and control studies.

The present paper addresses this gap by applying balanced truncation to a linearized dq frame model of an islanded microgrid benchmark that includes two micro sources, two inverters, and two RLC loads [22]. The benchmark model in the study [22] has fourteen states, four control inputs, and four output voltages at a nominal frequency of fifty hertz. Balanced truncation is used to construct reduced models with orders from one to thirteen. The analysis focuses on orders four and eight and evaluates H infinity norms for each input output channel as well as impulse responses and Bode plots. The results show that some output voltages are much more sensitive to truncation and that the eight-state model offers a good compromise between simplicity and fidelity. These findings provide a quantitative guideline for selecting reduced order models in multi-inverter microgrid applications where accurate dynamic behavior and manageable computational effort are both required.

2. MICROGRID SYSTEM MODEL

Figure 1 illustrates the structural diagram of an islanded microgrid system. In this system, two micro sources are integrated via inverters. Each micro source is connected to a Resistor-Inductor-Capacitor (RLC) load arranged in parallel at a common connection point. These loads are adjustable, allowing the simulation of standard electrical and electronic devices for testing and research purposes [22].

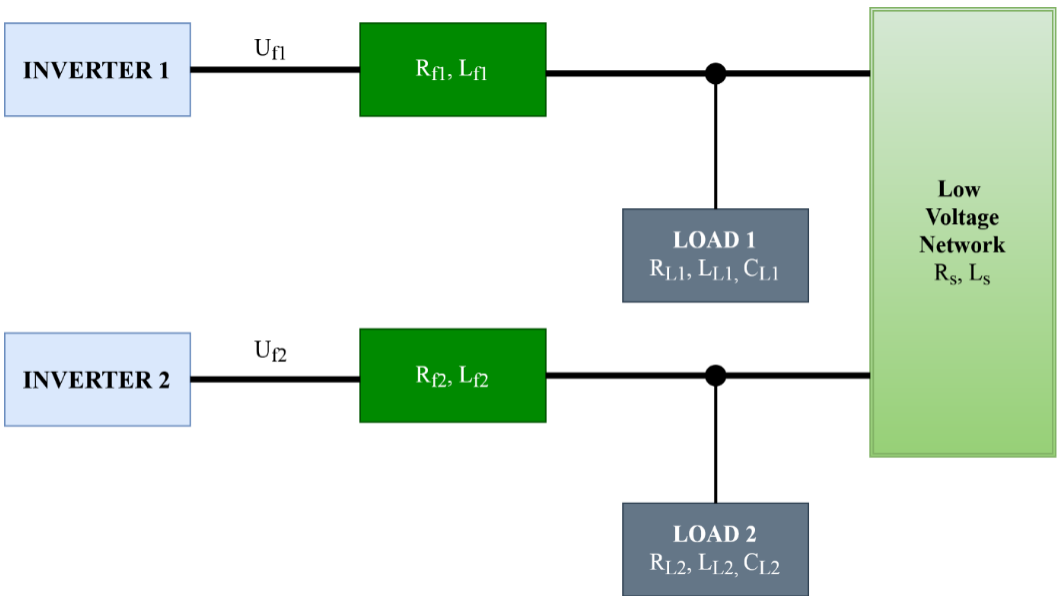

Figure 1. Islanded microgrid system model with structure consisting of two inverter sources

In islanded mode, the inverters are primarily controlled using a voltage-based control scheme to maintain the stability of the output voltage. These inverters are connected to the low-voltage grid through series filters composed of resistors and inductors. It is assumed that each micro source has the capability to dispatch power or is equipped with a sufficiently large storage system to maintain a stable DC voltage at the inverter's input. Additionally, the low-voltage grid is considered predominantly resistive, which simplifies the circuit modeling. Each inverter is connected to an individual load through a filter $Z_{f,i} = R_{f,i} + j\omega L_{f,i}$ with $i = 1, 2$ representing the inverter index. The loads are modeled as parallel RLC branches that can be adjusted to simulate standard electrical consumption devices.

Based on the diagram in Figure 1, we can derive the state equations of the microgrid system in a three-phase reference

frame by applying Kirchhoff's voltage and current laws. Specifically, the basic equations are as follows [22]:

Voltage across the inverter 1 filter:

$$R_{f1}I_{f1} + L_{f1}\frac{dI_{f1}}{dt} + U_1 - U_{f1} = 0 \quad (1)$$

Current at the Point of Common Coupling (PCC) of inverter 1:

$$I_{L1} + C_{L1}\frac{dU_1}{dt} + \frac{U_1}{R_{L1}} - I_{f1} = 0 \quad (2)$$

Voltage across the load of inverter 1:

$$U_1 - R_{L1}I_{L1} - L_{L1}\frac{dI_{L1}}{dt} = 0 \quad (3)$$

Voltage across the inverter 2 filter:

$$U_{f2} - R_{f2}I_{f2} - L_{f2}\frac{dI_{f2}}{dt} - U_2 = 0 \quad (4)$$

Current at the PCC of inverter 2:

$$I_{f2} - I_{L2} - C_{L2}\frac{dU_2}{dt} - \frac{U_2}{R_{L2}} = 0 \quad (5)$$

Voltage across the load of inverter 2:

$$U_2 - R_{L2}I_{L2} - L_{L2}\frac{dI_{L2}}{dt} = 0 \quad (6)$$

Current in the low voltage network:

$$U_1 - R_sI_s - L_s\frac{dI_s}{dt} - U_2 = 0 \quad (7)$$

$$\begin{bmatrix} u_d \\ u_q \\ u_0 \end{bmatrix} = \sqrt{\frac{2}{3}} \begin{bmatrix} \cos\alpha & \cos(\alpha - \frac{2\pi}{3}) & \cos(\alpha + \frac{2\pi}{3}) \\ -\sin\alpha & -\sin(\alpha - \frac{2\pi}{3}) & -\sin(\alpha + \frac{2\pi}{3}) \\ \frac{1}{\sqrt{2}} & \frac{1}{\sqrt{2}} & \frac{1}{\sqrt{2}} \end{bmatrix} \begin{bmatrix} u_a \\ u_b \\ u_c \end{bmatrix} \quad (8)$$

For the convenience of analysis and control, the above equations are transformed from three-phase quantities into the dq frame using a transformation matrix. Here, $\alpha = \omega t$ is the rotating phase angle with angular frequency ω. After transformation, the state equations of the three-phase system in the dq frame are expressed as follows Eq. (8).

Voltage across the inverter 1 filter:

$$\frac{di_{f1}}{dt} + j\omega i_{f1} + \frac{1}{L_{f1}}u_1 + \frac{R_{f1}}{L_{f1}}i_{f1} - \frac{1}{L_{f1}}u_{f1} = 0 \quad (9)$$

Current at the PCC for inverter 1:

$$\frac{du_1}{dt} + j\omega u_1 + \frac{1}{R_{L1}C_{L1}}u_1 + \frac{1}{C_{L1}}i_{L1} + \frac{1}{C_{L1}}i_s - \frac{1}{C_{L1}}i_{f1} = 0 \quad (10)$$

Voltage across the inverter 1 load:

$$\frac{di_{L1}}{dt} + j\omega i_{L1} + \frac{R_{L1}}{L_{L1}}i_{L1} - \frac{1}{L_{L1}}u_1 = 0 \quad (11)$$

Voltage across the inverter 2 filter:

$$\frac{di_{f2}}{dt} + j\omega i_{f2} + \frac{R_{f2}}{L_{f2}}i_{f2} - \frac{1}{L_{f2}}u_{f2} = 0 \quad (12)$$

Current at the PCC for inverter 2:

$$\frac{du_2}{dt} + j\omega u_2 + \frac{1}{R_{L2}C_{L2}}u_2 + \frac{1}{C_{L2}}i_{L2} + \frac{1}{C_{L2}}i_s - \frac{1}{C_{L2}}i_{f2} = 0 \quad (13)$$

Voltage across the inverter 2 load:

$$\frac{di_{L2}}{dt} + j\omega i_{L2} + \frac{1}{L_{L2}}u_2 + \frac{R_{L2}}{L_{L2}}i_{L2} - \frac{1}{L_{L2}}u_{t2} = 0 \quad (14)$$

The equation describes the current through the connection between two inverters:

$$\frac{di_s}{dt} + j\omega i_s = -\frac{R_s}{L_s}i_s + \frac{1}{L_s}u_1 - \frac{1}{L_s}u_2 \quad (15)$$

Model $f(x,u) = 0 \Rightarrow \Delta\dot{x} = A\Delta x + B\Delta u$, linearized at $V = 1$, p.u., $f = 50$, Hz, $P_1 = P_2 \approx$ cons. After combining the state equations of both inverters in the dq frame, a 14th-order state-space model is obtained. The vector x(t) consists of 14 state variables corresponding to the current and voltage components in the dq frame of the two inverters and the low voltage network, the vector u(t) comprises 4 components representing the control voltages from the inverters, and the vector y(t) comprises 4 components representing the load voltages in the dq frame are defined as follows:

$$\begin{cases} \dot{x}(t) = Ax(t) + Bu(t) \\ y(t) = Cx(t) + Du(t) \end{cases} \quad (16)$$

where, A is the state coefficient matrix; B is the input matrix; C is the output matrix; D is the direct transmission matrix [22].

$$B^T = \begin{bmatrix} \frac{1}{L_{f1}} & 0 & 0 & 0 & 0 & 0 & 0 & 0 & 0 & 0 & 0 & 0 & 0 & 0 \\ 0 & \frac{1}{L_{f1}} & 0 & 0 & 0 & 0 & 0 & 0 & 0 & 0 & 0 & 0 & 0 & 0 \\ 0 & 0 & 0 & 0 & 0 & 0 & 0 & 0 & \frac{1}{L_{f2}} & 0 & 0 & 0 & 0 & 0 \\ 0 & 0 & 0 & 0 & 0 & 0 & 0 & 0 & 0 & \frac{1}{L_{f2}} & 0 & 0 & 0 & 0 \end{bmatrix}$$

$$C = \begin{bmatrix} 0 & 0 & 1 & 0 & 0 & 0 & 0 & 0 & 0 & 0 & 0 & 0 & 0 & 0 \\ 0 & 0 & 0 & 1 & 0 & 0 & 0 & 0 & 0 & 0 & 0 & 0 & 0 & 0 \\ 0 & 0 & 0 & 0 & 0 & 0 & 0 & 0 & 0 & 0 & 1 & 0 & 0 & 0 \\ 0 & 0 & 0 & 0 & 0 & 0 & 0 & 0 & 0 & 0 & 0 & 1 & 0 & 0 \end{bmatrix};$$

$$D = \begin{bmatrix} 0 & 0 & 0 & 0 \\ 0 & 0 & 0 & 0 \\ 0 & 0 & 0 & 0 \\ 0 & 0 & 0 & 0 \end{bmatrix}$$

Table 1 summarizes the parameters and values of the microgrid system. These parameters include resistances, inductances, and capacitances for the inverters, low-voltage networks, and loads [22]. The table provides a clear overview of the system components and their characteristics.

Table 1. Microgrid system parameters and values

Component	Parameter	Value	Description
Inverter Filter 1	R_{f1}	1.5 mΩ	Resistance of inverter 1 filter
	L_{f1}	300 μH	Inductance of inverter 1 filter
Inverter Filter 2	R_{f2}	8 mΩ	Resistance of inverter 2 filter
	L_{f2}	900 μH	Inductance of inverter 2 filter
LV Network	R_s	1 Ω	Resistance of LV network
	L_s	100 mH	Inductance of LV network
Load 1	R_{L1}	58 Ω	Resistance of load 1
	L_{L1}	113.8 mH	Inductance of load 1
	C_{L1}	84.8 μF	Capacitance of load 1
Load 2	R_{L2}	100 Ω	Resistance of load 2
	L_{L2}	200 mH	Inductance of load 2
	C_{L2}	67 μF	Capacitance of load 2

$$A = \begin{bmatrix} -\frac{R_{f1}}{L_{f1}} & \omega & 0 & 0 & 0 & 0 & 0 & 0 & 0 & 0 & 0 & 0 & \frac{1}{L_{f1}} & 0 \\ -\omega & -\frac{R_{f1}}{L_{f1}} & 0 & 0 & 0 & 0 & 0 & 0 & 0 & 0 & 0 & 0 & 0 & \frac{1}{L_{f1}} \\ \frac{1}{C_{L1}} & 0 & 0 & \omega & -\frac{1}{C_{L1}} & 0 & 0 & 0 & 0 & 0 & 0 & 0 & 0 & 0 \\ 0 & \frac{1}{C_{L1}} & -\omega & 0 & 0 & -\frac{1}{C_{L1}} & 0 & 0 & 0 & 0 & 0 & 0 & 0 & 0 \\ 0 & 0 & \frac{1}{L_{L1}} & 0 & -\frac{R_{L1}}{L_{L1}} & \omega & 0 & 0 & 0 & 0 & 0 & 0 & 0 & 0 \\ 0 & 0 & 0 & \frac{1}{L_{L1}} & -\omega & -\frac{R_{L1}}{L_{L1}} & 0 & 0 & 0 & 0 & 0 & 0 & 0 & 0 \\ 0 & 0 & 0 & 0 & 0 & 0 & -\frac{R_s}{L_s} & \omega & -\frac{1}{L_s} & 0 & \frac{1}{L_s} & 0 & 0 & 0 \\ 0 & 0 & 0 & 0 & 0 & 0 & -\omega & -\frac{R_s}{L_s} & 0 & -\frac{1}{L_s} & 0 & \frac{1}{L_s} & 0 & 0 \\ 0 & 0 & 0 & 0 & 0 & 0 & 0 & 0 & -\frac{R_{L2}}{L_{L2}} & \omega & -\frac{1}{L_{L2}} & 0 & \frac{1}{L_{L2}} & 0 \\ 0 & 0 & 0 & 0 & 0 & 0 & 0 & 0 & -\omega & -\frac{R_{L2}}{L_{L2}} & 0 & -\frac{1}{L_{L2}} & 0 & \frac{1}{L_{L2}} \\ 0 & 0 & 0 & 0 & 0 & 0 & \frac{1}{C_{L2}} & 0 & 0 & 0 & 0 & \omega & -\frac{1}{C_{L2}} & 0 \\ 0 & 0 & 0 & 0 & 0 & 0 & 0 & \frac{1}{C_{L2}} & 0 & 0 & -\omega & 0 & 0 & -\frac{1}{C_{L2}} \\ 0 & 0 & 0 & 0 & 0 & 0 & 0 & 0 & 0 & 0 & \frac{1}{L_{f2}} & 0 & -\frac{R_{f2}}{L_{f2}} & \omega \\ 0 & 0 & 0 & 0 & 0 & 0 & 0 & 0 & 0 & 0 & 0 & \frac{1}{L_{f2}} & -\omega & -\frac{R_{f2}}{L_{f2}} \end{bmatrix}$$

3. BALANCED TRUNCATION MODEL ORDER REDUCTION TECHNIQUE

Balanced truncation is a classical model order reduction method in control engineering that produces a balanced realization of the state space model [13]. In this realization, the controllability Gramian and the observability Gramian are equal and diagonal and the diagonal entries are the Hankel singular values. States with small Hankel singular values have a limited impact on the input to output behavior so they can be removed while the main dynamics remain. The present work follows the standard balanced truncation procedure and the Lyapunov equations, Gramian factorizations, singular value decomposition, state transformation and truncation steps are given in Eqs. (17) to (24):

$$PA^T + BB^T + AP = 0 \tag{17}$$

$$QA + C^TC + A^TQ = 0 \tag{18}$$

$$P = chol(R)^T \tag{19}$$

$$Q = chol(L)^T \tag{20}$$

$$L^TR = VSU^T \tag{21}$$

$$T = S^{-1/2}V^TL^T; T^{-1} = RUS^{-1/2} \tag{22}$$

$$S = \begin{bmatrix} S_r & 0 \\ 0 & S_{rem} \end{bmatrix} \tag{23}$$

$$\tilde{A} = \begin{bmatrix} A_{11} & A_{12} \\ A_{21} & A_{22} \end{bmatrix}, \tilde{B} = \begin{bmatrix} B_1 \\ B_2 \end{bmatrix}, \tilde{C} = [C_1 \quad C_2] \tag{24}$$

The reduced-order model is then obtained by retaining the blocks A_{11}, B_1, C_1.

By truncating the states with negligible contributions, balanced truncation ensures that the reduced-order model retains the key characteristics of the original system while minimizing the error between their outputs.

4. RESULTS AND DISCUSSION

A reduction of the microgrid model from fourteen states down to order one yields a family of reduced systems whose H_∞ errors vary with the retained order, as shown in Figures 2 to 5. For order one, the errors are very large for channels from Inputs 1 and 2 to Outputs 1 and 2, with values around 33.39 and 17.89, while the errors related to Inputs 3 and 4 remain near 0.058. Orders two and three still exhibit non-uniform behavior since errors for Outputs 1 and 2 decrease only gradually, and some channels that involve Outputs 3 and 4 keep values above 14. At order four, the errors for channels that terminate at Outputs 1 and 2 fall to about 0.0012 while errors for channels that terminate at Outputs 3 and 4 stay near 14.5. Orders five to seven show irregular patterns in which several channels reach values in the range of 10 to 30, while others already move into the range of 10 to the power of minus three. Order eight marks a turning point because the errors for all input-output pairs fall into a narrow band between 0.000318 and 0.002189. Orders nine to thirteen keep the errors at low levels with small variations that do not change the qualitative picture.

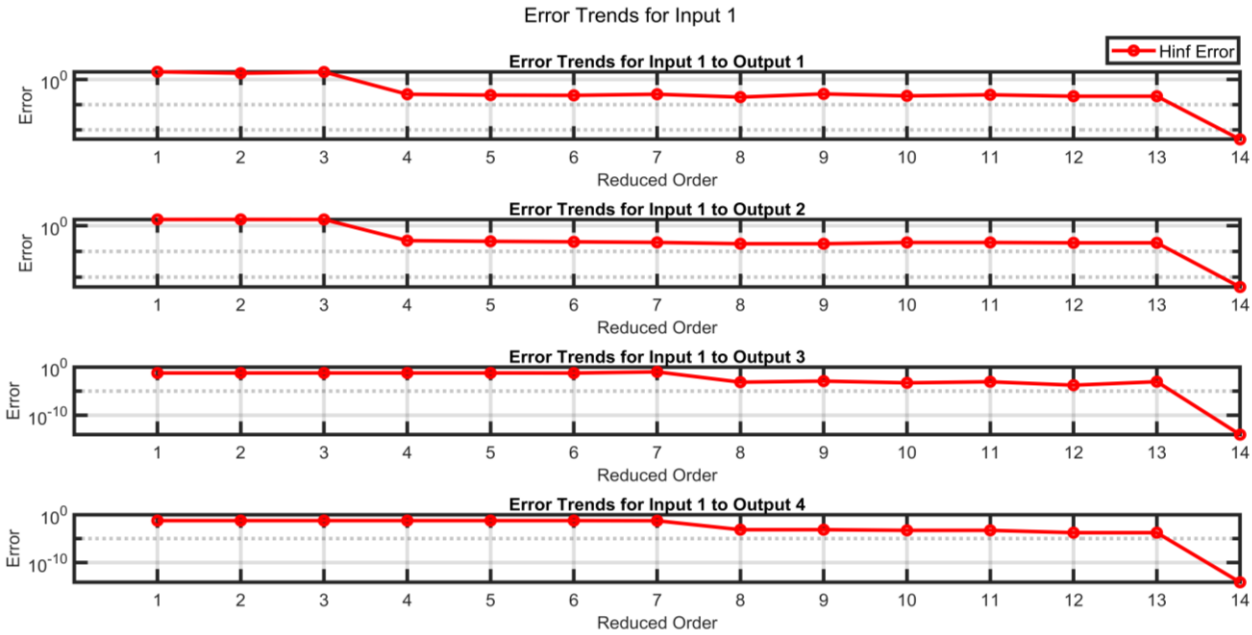

Figure 2. H_∞ error plot from Input 1 to the four outputs

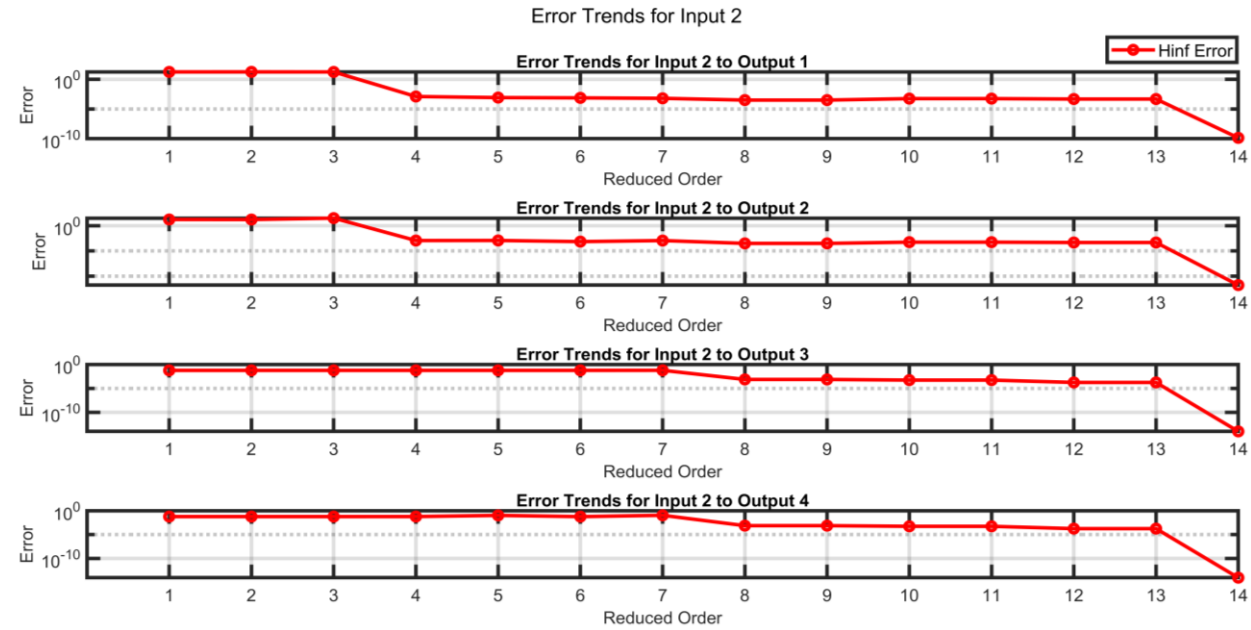

Figure 3. H_∞ error plot from Input 2 to the four outputs

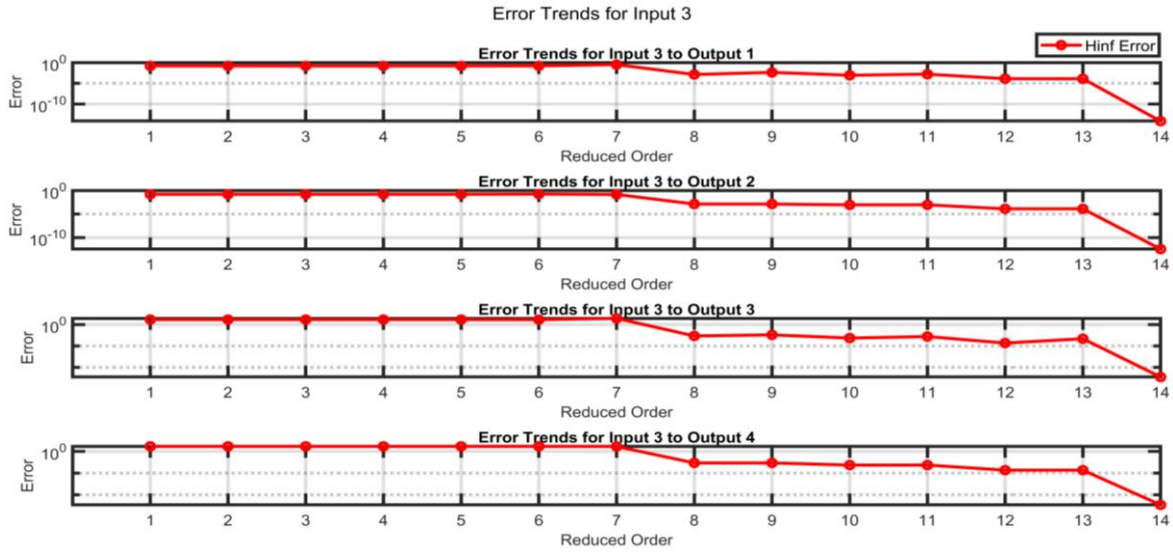

Figure 4. H_∞ error plot from Input 3 to the four outputs

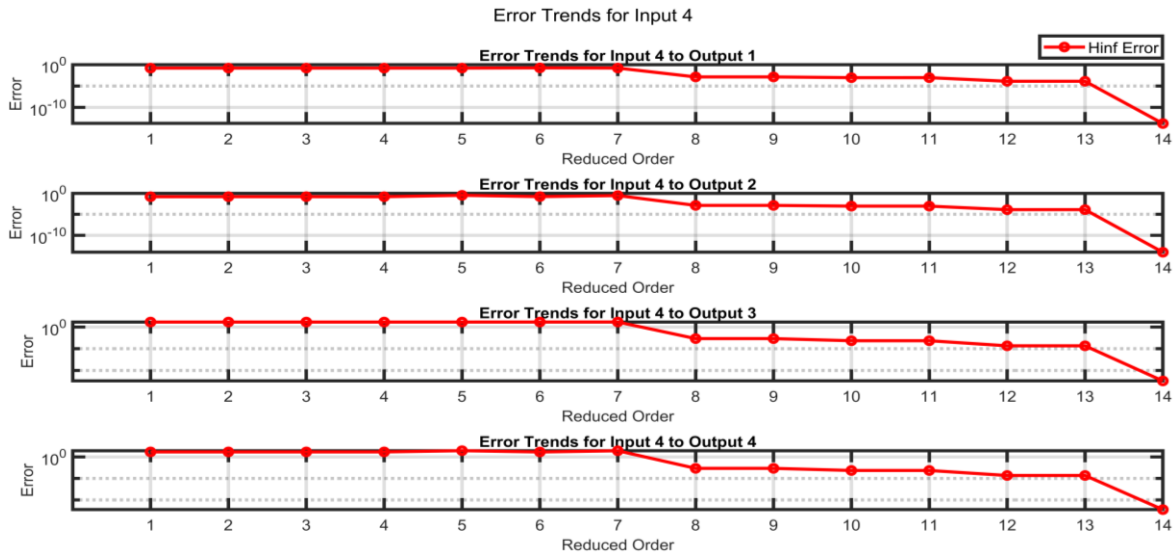

Figure 5. H_∞ error plot from Input 4 to the four outputs

Table 2. H_∞ error matrix for reduced order r = 4

Component	Input 1	Input 2	Input 3	Input 4
Output 1	0.001168	0.001266	0.059077	0.057463
Output 2	0.001266	0.001168	0.057463	0.059077
Output 3	0.157201	0.154186	14.764552	14.447584
Output 4	0.154186	0.157201	14.447584	14.764554

The detailed H_∞ error matrix for order four in Table 2 confirms that channels associated with Outputs 1 and 2 behave very differently from channels associated with Outputs 3 and 4. For Inputs 1 and 2, the errors to Outputs 1 and 2 are close to 0.001,2, while the errors to Outputs 3 and 4 stay near 0.15. For Inputs 3 and 4, the errors to Outputs 1 and 2 are around 0.058, while the errors to Outputs 3 and 4 are about 14.7. Impulse responses in Figures 6 to 9 illustrate the same pattern. Channels from Inputs 1 and 2 to Outputs 1 and 2 show almost indistinguishable transients and steady state behavior between the order four and full order models. Channels that involve Outputs 3 and 4 show visible deviations during the transient interval and converge only in the steady state region. The magnitude and phase plots in Figures 10 to 13 reinforce this observation. Channels from Inputs 1 and 2 to Outputs 1 and 2 display very close magnitude and phase curves across the studied frequency range, while channels that involve Outputs 3 and 4 show noticeable differences at higher frequencies. For Inputs 3 and 4, the magnitude curves in Figure 12 agree well with the full order model below about ten to the power of four radians per second, while larger discrepancies appear at higher frequencies and across multiple bands for channels that end at Outputs 3 and 4. Phase responses in Figure 13 differ over most of the frequency range for channels that originate from Inputs 3 and 4, which indicates that the order four model is not suitable when accurate phase information is needed on those paths.

The H_∞ error matrix for order eight in Table 3 shows a different picture. All channels now have errors between 0.000318 and 0.002189. Channels that involve Outputs 1 and 2 lie near the lower end of this band, and channels that involve Outputs 3 and 4 lie near the upper end, yet still remain very small. Impulse responses in Figures 14 to 17 show an almost exact match between the order eight and full order models for all input-output pairs across the entire time axis. The reduced model captures both the transient overshoots and the settling behavior without visible distortion. Magnitude plots in Figures 18 and 20 reveal very small differences over most of the

frequency range. For Inputs 1 and 2, the magnitude curves are practically identical for Outputs 1 and 2 and stay very close for Outputs 3 and 4 up to about ten to the power of five radians per second. For Inputs 3 and 4, the magnitude agreement is very good for Outputs 3 and 4 and remains acceptable for Outputs 1 and 2 in the same frequency band. Phase plots in Figures 19 and 21 display small deviations that become visible at higher frequencies yet remain limited in size. Channels from Input 1 to Output 2 and from Input 3 to Output 4 show almost coincident phase traces, which suggests that the order eight model can replace the full order model for phase-related studies on these paths.

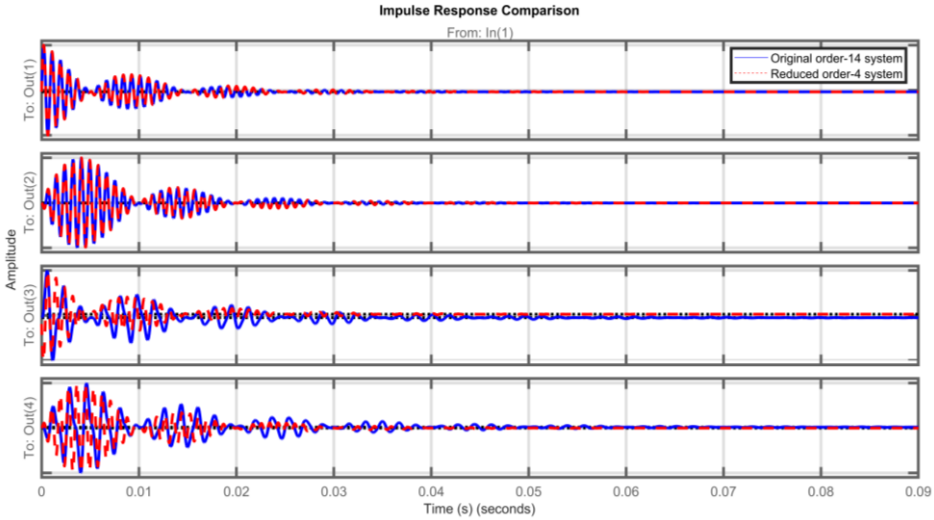

Figure 6. Impulse response of the r = 4 reduced model and the full-order model for Inputs 1 to 4

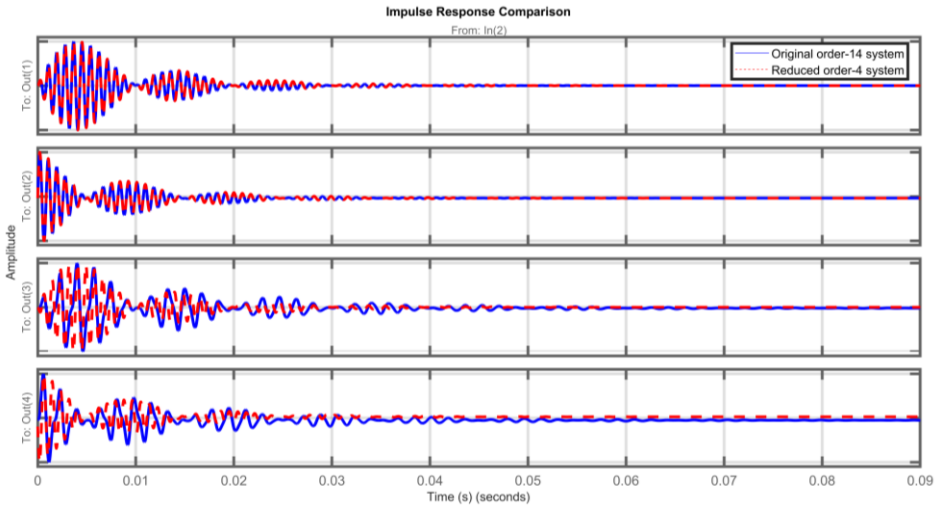

Figure 7. Impulse response of the r = 4 reduced model and the full-order model for Inputs 2 to 4

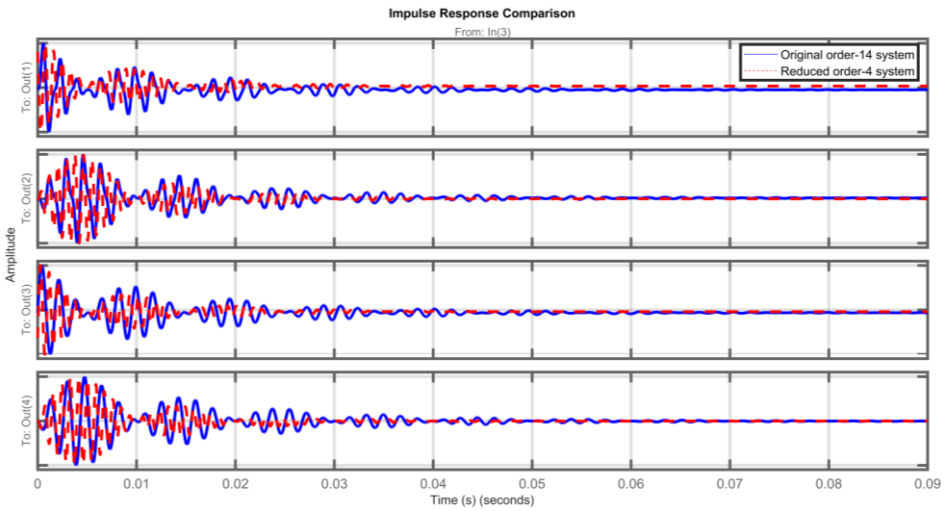

Figure 8. Impulse response of the r = 4 reduced model and the full-order model for Inputs 3 to 4

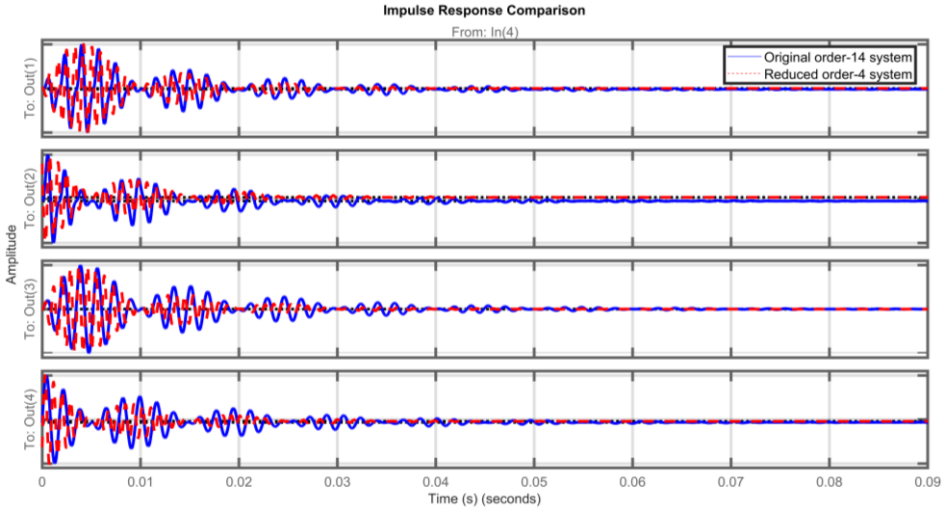

Figure 9. Impulse response of the r = 4 reduced model and the full-order model for Input 4 to 4 outputs

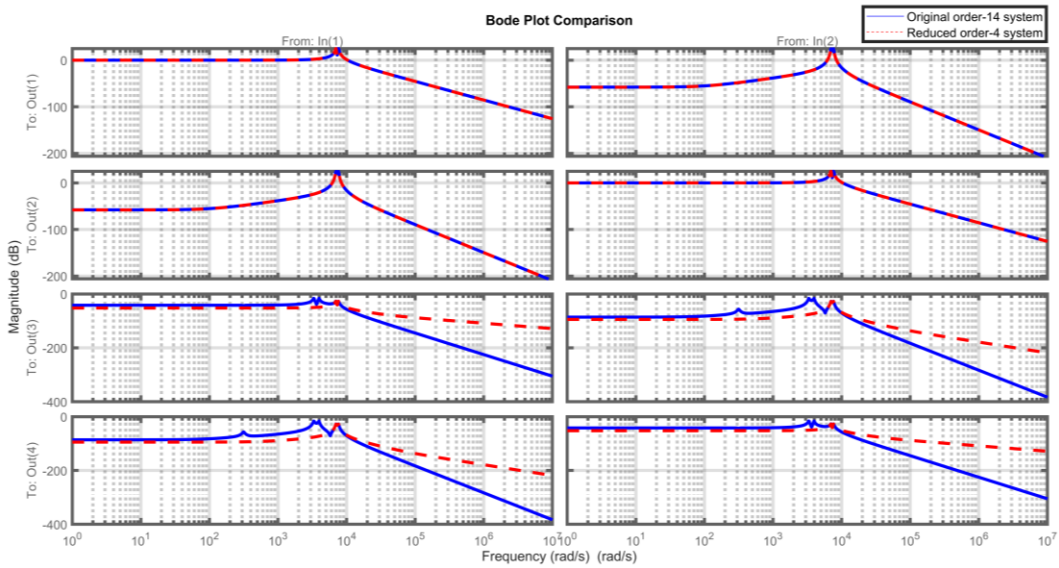

Figure 10. Magnitude response of the r = 4 reduced model and the full-order model from Inputs 1 and 2 to 4 outputs

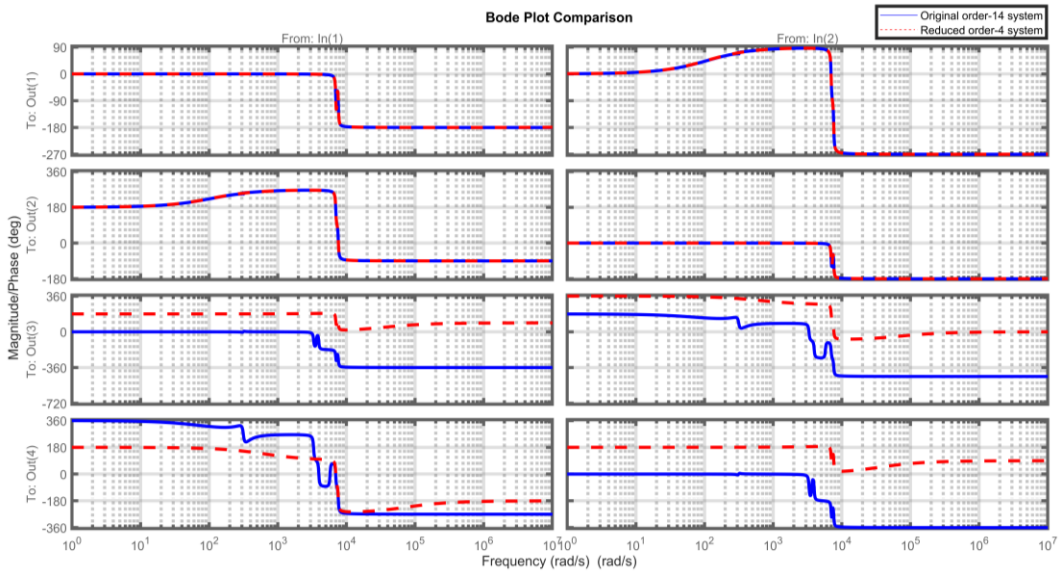

Figure 11. Phase response of the r = 4 reduced model and the full-order model from Inputs 1 and 2 to 4 outputs

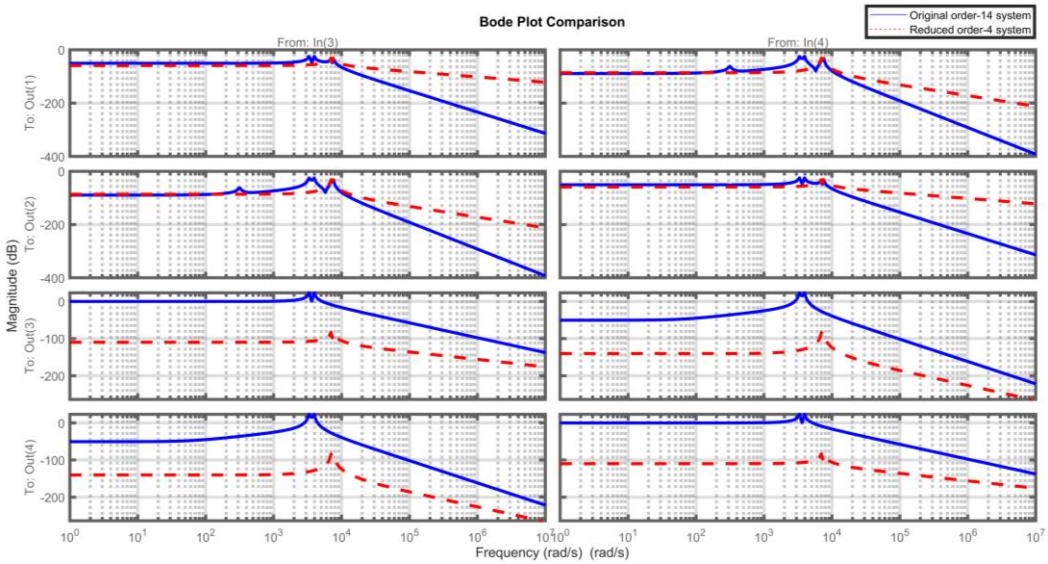

Figure 12. Magnitude response of the r = 4 reduced model and the full-order model from Inputs 3 and 4 to 4 outputs

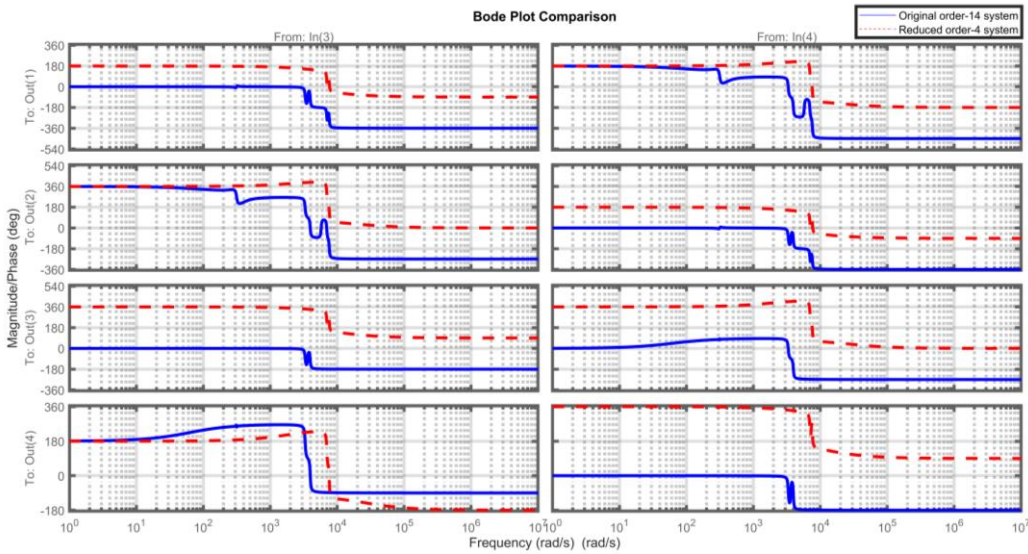

Figure 13. Phase response of the r = 4 reduced model and the full-order model from Inputs 3 and 4 to 4 outputs

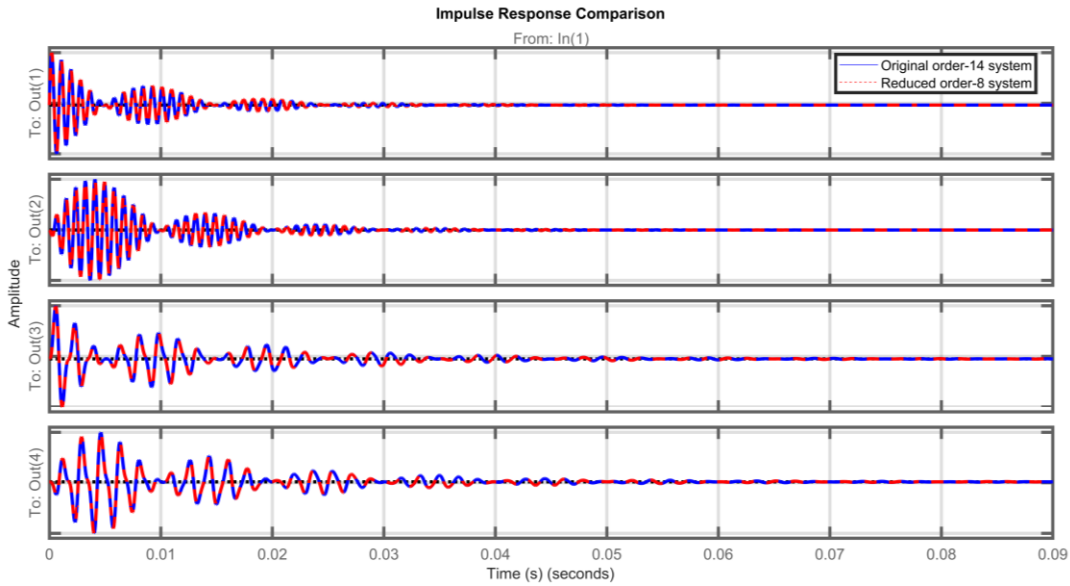

Figure 14. Impulse response of the r = 8 reduced model and the full-order model for Inputs 1 to 4

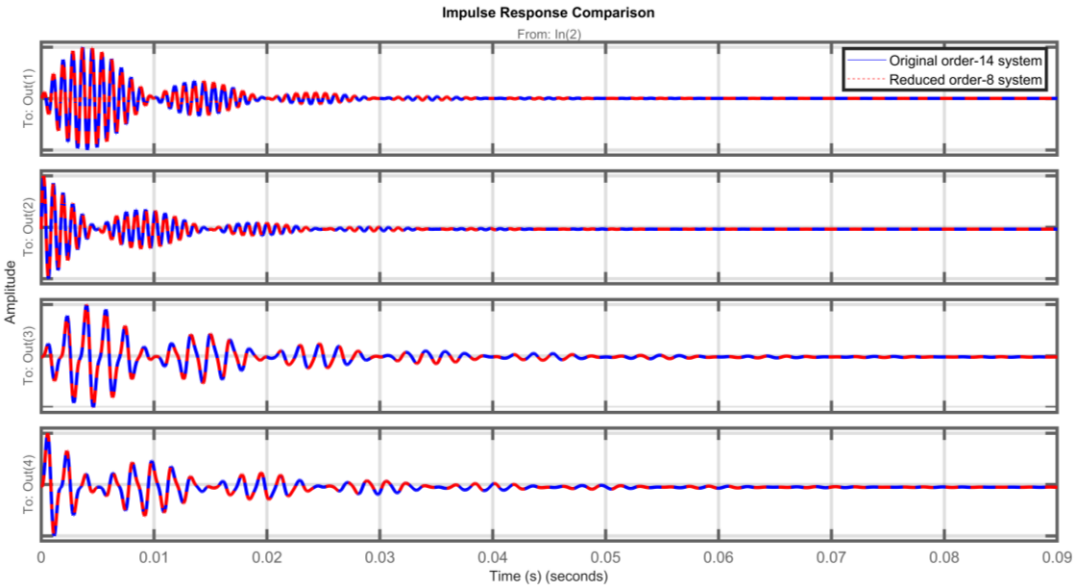

Figure 15. Impulse response of the r = 8 reduced model and the full-order model for Inputs 2 to 4

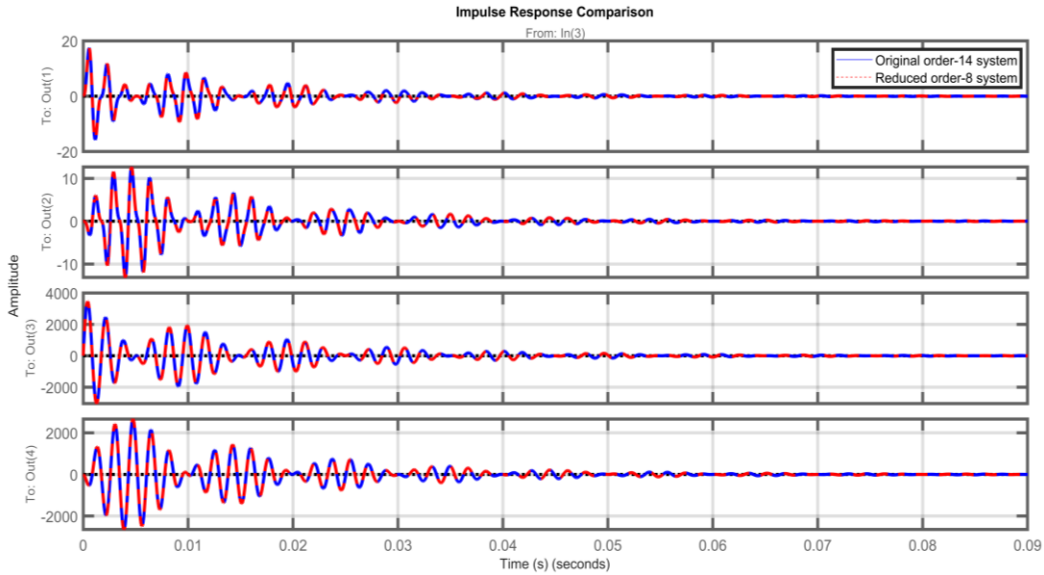

Figure 16. Impulse response of the r = 8 reduced model and the full-order model for Inputs 3 to 4

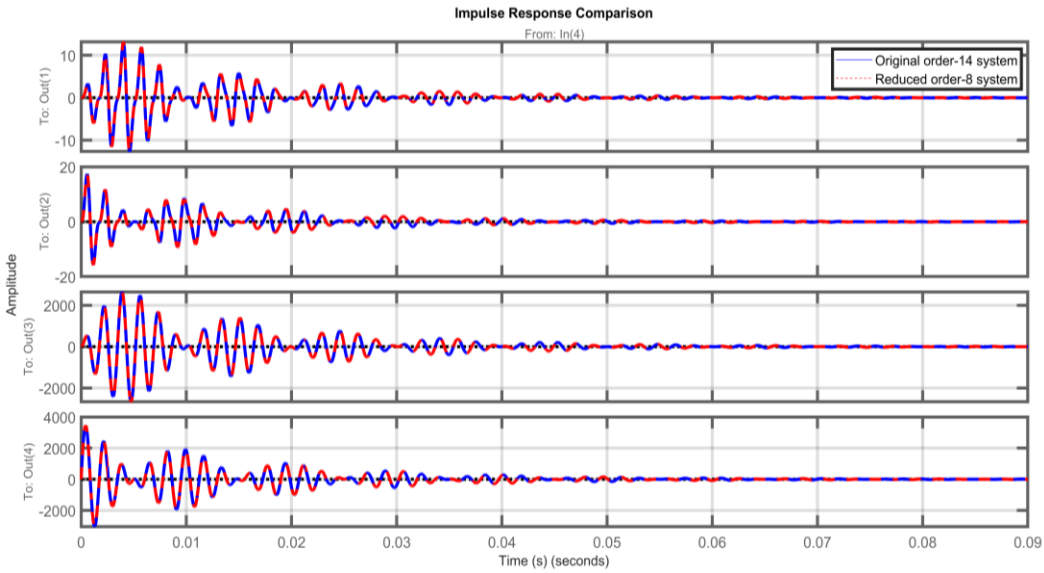

Figure 17. Impulse response of the r = 8 reduced model and the full-order model for Input 4 to 4 outputs

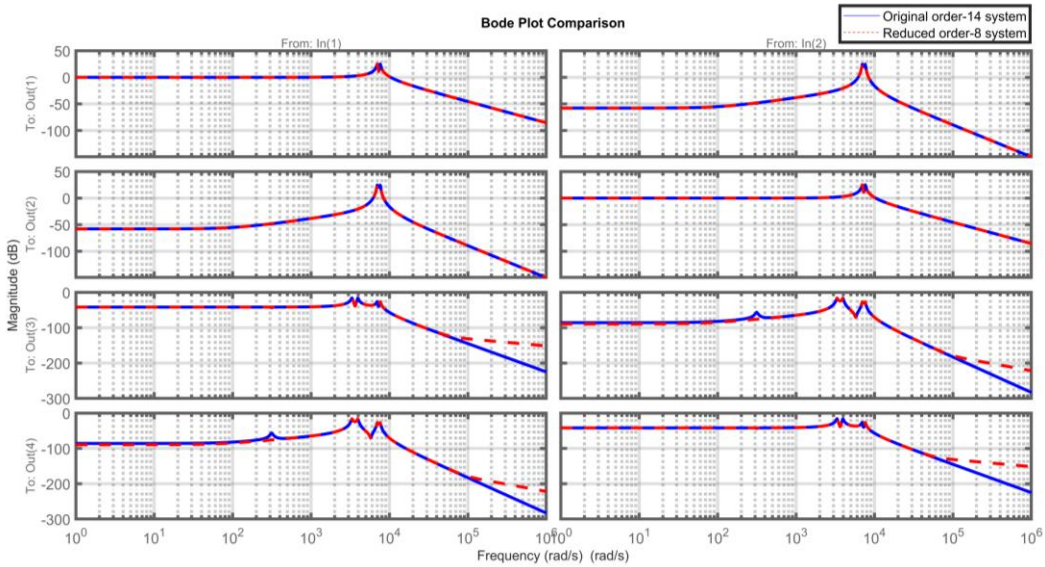

Figure 18. Magnitude response of the r = 8 reduced model and the full-order model from Inputs 1 and 2 to 4 outputs

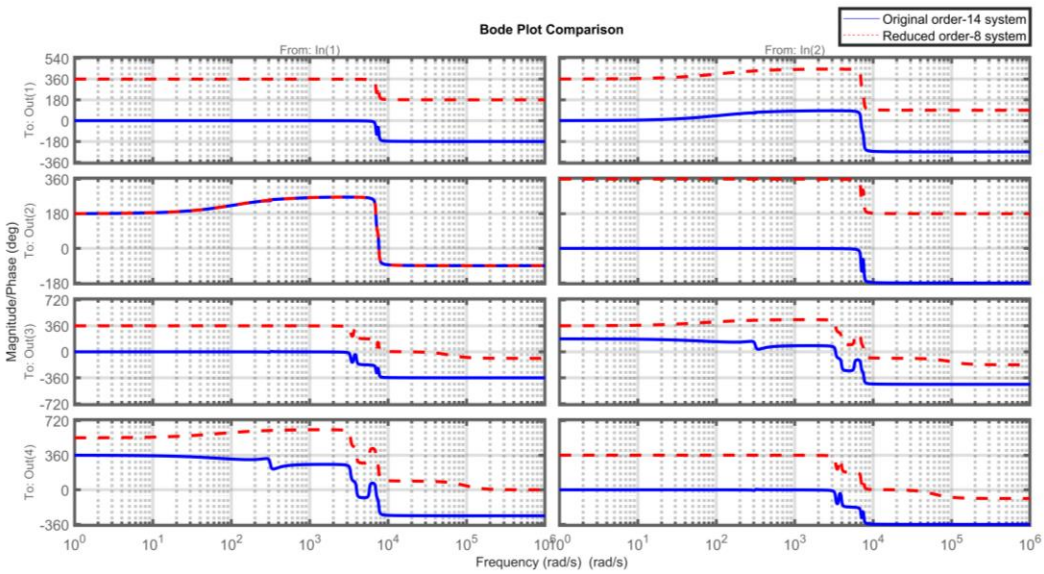

Figure 19. Phase response of the r = 8 reduced model and the full-order model from Inputs 1 and 2 to 4 outputs

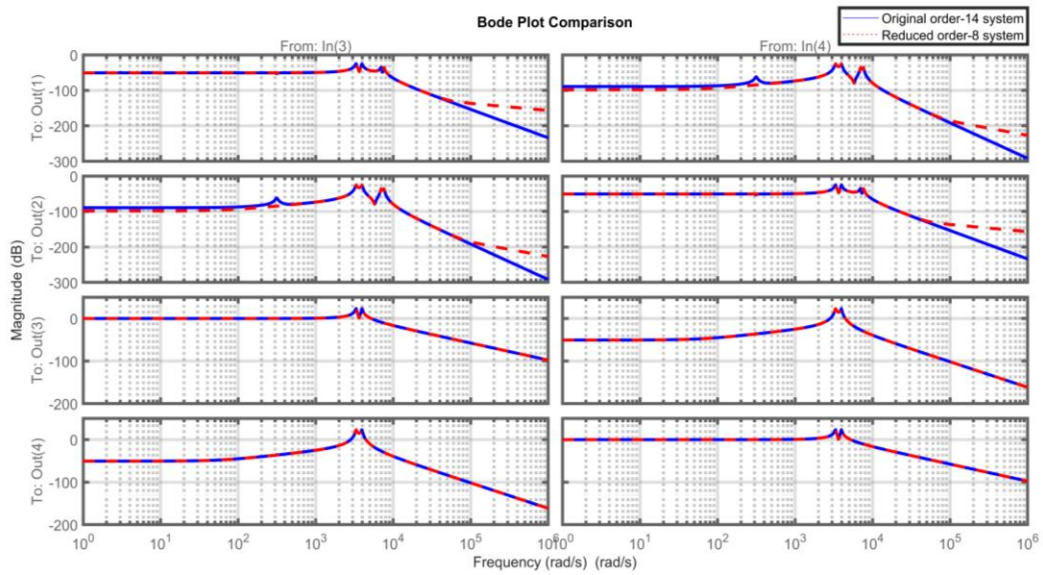

Figure 20. Magnitude response of the r = 8 reduced model and the full-order model from Inputs 3 and 4 to 4 outputs

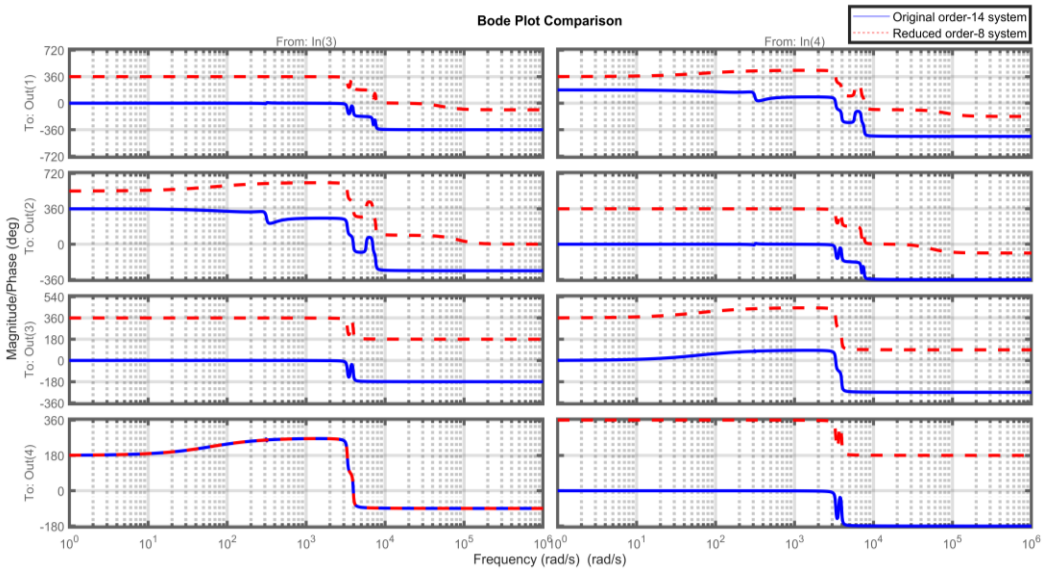

Figure 21. Phase response of the r = 8 reduced model and the full-order model from Inputs 3 and 4 to 4 outputs

Table 3. H_∞ error matrix for reduced order r = 8

Component	Input 1	Input 2	Input 3	Input 4
Output 1	0.000318	0.000318	0.000740	0.000740
Output 2	0.000318	0.000318	0.000740	0.000740
Output 3	0.001331	0.001331	0.002188	0.002189
Output 4	0.001331	0.001331	0.002189	0.002188

A comparison of the two reduced orders indicates a clear trade-off between simplicity and fidelity. The order four model preserves the dominant dynamics for channels associated with Outputs 1 and 2, which makes it attractive when the study focuses on those buses, and a compact representation is desired. The same model fails to represent channels that involve Outputs 3 and 4 due to the removal of states that are important for the remote part of the network. The order eight model retains the dominant modes for all outputs and achieves uniformly low H infinity errors, so it is better suited for applications that require accurate behavior across the entire set of input-output channels.

Impulse and Bode responses provide insight into the root cause of the different sensitivity between outputs. Outputs 3 and 4 correspond to buses that lie further from the inverters and are strongly shaped by the second RLC load and the line impedance. The states that describe these elements have smaller Hankel singular values than the states that dominate Outputs 1 and 2. Balanced truncation with order four discards part of the contribution from these weaker yet still relevant modes, which leads to large H infinity errors in channels that terminate at Outputs 3 and 4, even when channels related to Outputs 1 and 2 remain accurate. Balanced truncation with order eight keeps the leading modes associated with all four outputs, so the errors for Outputs 3 and 4 fall into the same small range as the other channels. This behavior implies that voltage nodes located deeper in the microgrid and more influenced by RLC dynamics are more sensitive to order selection and should be treated with care when low-order models are used in control design and performance assessment.

5. CONCLUSIONS

This study examined balanced truncation applied to a fourteen-state multiple-input multiple-output microgrid model and showed how the choice of reduced order shapes accuracy across individual input-output channels. The analysis of H infinity errors, impulse responses, and Bode plots indicates that a four-state model captures the dominant dynamics at the buses associated with the first two outputs but fails to represent satisfactorily the behavior at the more remote buses that define the third and fourth outputs. An eight-state model preserves the main modes that govern all four output voltages and achieves small and nearly uniform errors, so it offers a practical balance between model simplicity and fidelity.

The results highlight an important qualitative insight for microgrid applications. Voltage nodes located farther from the inverters and strongly influenced by RLC elements are more sensitive to state reduction than nodes that lie closer to the sources. Reduced models that are acceptable for studies focused on local buses may not be adequate when the analysis or controller design requires accurate behavior across the full network. The work provides a quantitative guideline for selecting reduced orders in such cases since it links order choice, channel-wise H infinity errors, and time and frequency domain responses.

The present model relies on a linear time-invariant representation obtained by linearizing the microgrid dynamics around a single operating point, and the study considers only a standard balanced truncation procedure. Nonlinear effects, operating point variation, and parameter uncertainty are not captured explicitly, so the conclusions apply to a restricted yet practically relevant class of operating conditions. The evaluation is based on simulation rather than experimental data and does not include implementation aspects in embedded platforms.

Future research can extend this framework in several directions. One promising line is to explore balanced truncation within nonlinear or parameter-dependent formulations that track changes in loading and generation. Another is to combine balanced truncation with other model order reduction techniques in hybrid schemes tailored to microgrids, such as positive real variants or mixed energy-based approaches. Real-time capable reduced models integrated in hardware in the loop setups and experimental validation on laboratory microgrids would further test the robustness and practical value of the proposed guideline for

order selection.

ACKNOWLEDGMENT

The author gratefully acknowledges the support of the Thai Nguyen University of Technology and the Education Technology and Adaptive Learning Institute, Thai Nguyen University of Technology, Vietnam.

REFERENCES

[1] Setiabudy, R., Setiawan, E.A., Sudibyo, U.B. (2011). Development of direct current microgrid control for ensuring power supply from renewable energy sources. International Journal of Technology, 2(3): 199-206.

[2] Onibonoje, M.O., Alegbeleye, O.O., Ojo, A.O. (2023). Control design and management of a distributed energy resources system. International Journal of Technology, 14(2): 236-245. https://doi.org/10.14716/ijtech.v14i2.5884

[3] Mishra, A., Gundavarapu, V.N.K. (2018). Disparity line utilization factor and galaxy-based search algorithm for advanced congestion management in power systems. International Journal of Technology, 7(1): 88-96. https://doi.org/10.14716/ijtech.v7i1.1556

[4] Khoirunisa, R., Mushfiroh, A., Gamal, A. (2023). The identification of challenges in innovation ecosystem of West Java, Indonesia using a systematic literature review. International Journal of Technology, 14(7): 1408-1418. https://doi.org/10.14716/ijtech.v14i7.6662

[5] Attia, H., Suan, S.T.K. (2024). Robust sliding mode controller design for boost converter applications. International Journal of Technology, 15(3): 481-491. https://doi.org/10.14716/ijtech.v15i3.5164

[6] Purwo Sutikno, J., Azizah, Z., Handogo, R., Aris Hikmadiyar, R., Hisyam, A. (2019). Inverted decoupling 2DoF internal model control for MIMO processes. International Journal of Technology, 10(3): 502-511. https://doi.org/10.14716/ijtech.v10i3.2922

[7] Khazimov, K., Sagyndykova, Z., Khazimov, Z., Daurenova, I., Umbetkulov, Y., Khazimov, M. (2024). Thermal welding in the neck of vacuum flexible container with self-propelled welding module. International Journal of Technology, 15(4): 1088-1101. https://doi.org/10.14716/ijtech.v15i4.6486

[8] Arifin, A.S., Ohtsuki, T. (2015). Ergodic capacity analysis of full-duplex MIMO relay channel using Tracy-Widom distribution with processing delay. International Journal of Technology, 6(2): 151-159. https://doi.org/10.14716/ijtech.v6i2.1003

[9] Utama, D.M., Yurifah, A., Garside, A.K. (2023). A novel hybrid spotted hyena optimizer: An algorithm for fuel consumption capacitated vehicle routing problem. International Journal of Technology, 14(5): 1049-1059. https://doi.org/10.14716/ijtech.v14i5.5148

[10] Alwan, H.M., Nikolaevic, V.A., Hasan, S.F., Vladmerovna, K.O. (2024). Kinematic and dynamic modeling based on trajectory tracking control of mobile robot with Mecanum wheels. International Journal of Technology, 15(5): 1473-1486. https://doi.org/10.14716/ijtech.v15i5.6908

[11] Göthner, F., Roldán-Pérez, J., Torres-Olguin, R.E., Midtgård, O.M. (2022). Reduced-order model of distributed generators with internal loops and virtual impedance. IEEE Transactions on Smart Grid, 13(1): 119-128. https://doi.org/10.1109/TSG.2021.3120323

[12] Tonkens, S., Lorenzetti, J., Pavone, M. (2021). Soft robot optimal control via reduced order finite element models. In 2021 IEEE International Conference on Robotics and Automation (ICRA), Xi'an, China, pp. 12010-12016. https://doi.org/10.1109/ICRA48506.2021.9560999

[13] Le, L.H., Dang, D.C., Vu Phung, T.A., Nguyen, T.T.N. (2025). Applying the model order reduction based on the preservation of dominant poles to the robust control problem. Mathematical Modelling of Engineering Problems, 12(6): 1997-2004. https://doi.org/10.18280/mmep.120615

[14] Raj, T., Kumar, K., Jain, S. (2022). Reduced order model based design of linear active disturbance rejection controller with applications. In 2022 IEEE 7th International Conference for Convergence in Technology (I2CT), Mumbai, India, pp. 1-6. https://doi.org/10.1109/I2CT54291.2022.9824498

[15] Mushar, K., Hote, Y.V., Pillai, G.N. (2022). New mixed model order reduction approach for linear system. In 2022 IEEE International Conference on Signal Processing, Informatics, Communication and Energy Systems (SPICES), Thiruvananthapuram, India, pp. 343-348. https://doi.org/10.1109/SPICES52834.2022.9774083

[16] Kvasnicka, S., Roppert, K., Riener, C., Bauernfeind, T., Kaltenbacher, M. (2022). Model order reduction techniques for linear differential-algebraic equations applied to semi-discretized eddy current model. In 2022 IEEE 20th Biennial Conference on Electromagnetic Field Computation-Long Papers (CEFC-LONG), Denver, CO, USA, pp. 1-4. https://doi.org/10.1109/CEFC-LONG57069.2022.10107548

[17] Cheng, W., Li, Z., Li, Y., Chu, Y., et al. (2023). A model order reduction method considering the delay feature of wind power when participating in frequency regulation. In 2023 IEEE 6th Information Technology, Networking, Electronic and Automation Control Conference (ITNEC), Chongqing, China, pp. 737-743. https://doi.org/10.1109/ITNEC56291.2023.10082548

[18] Almasaabi, A., Varshney, T., Kakkar, S. (2023). Model order reduction of pressurized heavy water reactor: An overview. In 2023 International Conference on Recent Advances in Electrical, Electronics & Digital Healthcare Technologies (REEDCON), New Delhi, India, pp. 42-46. https://doi.org/10.1109/REEDCON57544.2023.10151149

[19] Chatzigeorgiou, C., Floros, G., Chatzigeorgiou, D., Evmorfopoulos, N., Stamoulis, G. (2024). Efficient parametric model order reduction for large-scale circuit models using extended Krylov subspace. In 2024 20th International Conference on Synthesis, Modeling, Analysis and Simulation Methods and Applications to Circuit Design (SMACD), Volos, Greece, pp. 1-4. https://doi.org/10.1109/SMACD61181.2024.10745437

[20] Rathore, S., Sharan, V., Kushwaha, S., Gupta, S. (2022). Model order reduction using Routh approximation and Pade method. In 2022 2nd International Conference on Advance Computing and Innovative Technologies in

Engineering (ICACITE), Greater Noida, India, pp. 2098-2102. https://doi.org/10.1109/ICACITE53722.2022.9823765

[21] Saiduzzaman, M., Shafiqul Islam, M., Bin Iqbal, K.I., Monir Uddin, M., Osman Gani, M. (2022). Frequency limited model reduction for large scale second-order index 1 system. In 2022 25th International Conference on Computer and Information Technology (ICCIT), Cox's Bazar, Bangladesh, pp. 893-896. https://doi.org/10.1109/ICCIT57492.2022.10054842

[22] Sen, S., Kumar, V. (2017). Assessment of various MOR techniques on an inverter-based microgrid model. In 2017 14th IEEE India Council International Conference (INDICON), Roorkee, India, pp. 1-6. https://doi.org/10.1109/INDICON.2017.8488052